OPEN ACCESS

Rashba effect at the surfaces of rare-earth metals and their monoxides

New Journal of Physics
The open-access journal for physics

Rashba effect at the surfaces of rare-earth metals and their monoxides

O Krupin[1,2,5], G Bihlmayer[3], K M Döbrich[1,6], J E Prieto[1,7], K Starke[1,8], S Gorovikov[4,9], S Blügel[3], S Kevan[2] and G Kaindl[1]

[1] Institut für Experimentalphysik, Freie Universität Berlin, Germany
[2] Department of Physics, University of Oregon, Eugene, OR, USA
[3] Institut für Festkörperforschung, Forschungszentrum Jülich, Germany
[4] MAX-Lab, Lund University, Sweden
E-mail: oleg.krupin@gmail.com

New Journal of Physics **11** (2009) 013035 (18pp)
Received 24 September 2008
Published 23 January 2009
Online at http://www.njp.org/
doi:10.1088/1367-2630/11/1/013035

Abstract. We present a systematic study of the Rashba-type spin–orbit interaction at the (0001) surfaces of rare-earth metals and their surface monoxides, specifically of Tb metal and the O/Tb, O/Lu and O/Y surfaces. By means of photoemission experiments and *ab initio* band-structure calculations, we uncover the influence of this interaction on the surface electronic structure. In turn, the dramatic impact of the charge-density distribution of the surface/interface states on the strength of the Rashba-type spin splitting is demonstrated. We discuss the Rashba effect at magnetic and non-magnetic rare-earth surfaces, and compare with cases where it is negligible. The difference between the Rashba effect and magnetic linear dichroism in photoemission is pointed out to help avoid possible confusion in connection with the simultaneous appearance of these two effects at a magnetic surface.

[5] Present address: Advanced Light Source, LBNL, USA.
[6] Present address: Max-Born-Instiut, Berlin, Germany.
[7] Present address: Centro de Microanálisis de Materiales and Instituto 'Nicolás Cabrera', Universidad Autónoma de Madrid, Spain.
[8] Deceased.
[9] Present address: Sincrotrone Trieste SCpA, Italy.

Contents

1. Introduction

Nowadays, spin-related phenomena are placed at the focus of research in solid-state physics aiming to develop a new branch of electronic technology often referred to as 'spintronics', where the spin degree of freedom of the electrons will be utilized in addition to the conventional manipulation of the electric charge. The electron spin is traditionally manipulated by applying a magnetic field, but electric-field control/manipulation of the spin is a key issue for spintronics devices. Spin control and manipulation by means of an electric field can be achieved through spin–orbit coupling [1]. In this context, the Rashba-type spin–orbit interaction has attracted considerable attention and several studies have been devoted to the investigation of the Rashba effect in semiconductor systems [2]–[5]. But only for a limited number of metallic surfaces/interfaces was this effect found to be large enough for direct spectroscopic observation [6]–[13].

The Hamiltonian describing the Rashba interaction can be written as

$$H_{\mathrm{R}} = \alpha(\vec{e}_z \times \vec{k}) \cdot \underline{\sigma}, \tag{1}$$

where the Rashba constant α is proportional to the effective electric field seen by the electron, the unit vector $\vec{e}_z$ is oriented perpendicular to the surface, $\vec{k}$ is the electron momentum and the spin is given by the Pauli matrices $\underline{\sigma}$. One expects maximal effects of the Rashba Hamiltonian when the electric field, the electron momentum and the electron spin are mutually orthogonal.

In two-dimensional (2D) systems with broken inversion symmetry, this spin–orbit interaction causes spin separation of the moving electrons. Inversion symmetry of the potential is naturally broken at any crystal surface or interface. This is why electronic states localized at a surface/interface should be spin split although this splitting can be vanishingly small. It was found that the Rashba interaction at crystal surfaces becomes sizeable only when it couples to the large intra-atomic spin–orbit interaction demonstrating that the gradient of the surface potential by itself is not sufficient to cause a directly observable splitting of the surface/interface electronic bands into spin subbands [6, 14]. Therefore, this interaction plays an important role only if high-Z elements are involved at the surfaces or interfaces.

The high Z-values of rare-earth (RE) metals suggest that the Rashba interaction should contribute significantly to their surface electronic structure. We have undertaken a systematic study of the electronic structure at the (0001) surfaces of Tb metal and of the O/Tb, O/Lu and O/Y systems, and we found indeed that spin–orbit interaction profoundly influences the electronic surface states at these surfaces. Surface states on clean surfaces of RE metals are not always easy to access with photoemission since they lie very close to the Fermi level and sometimes even above it [15, 16]. In contrast, the surface/interface states appearing on the (0001) surfaces of RE metals upon formation of surface monoxides are shifted to higher binding energies, i.e. they are below and well-separated from the Fermi level and are therefore an excellent choice for studies of Rashba interaction by photoemission [17].

The modification of the surface electronic structure caused by oxygen adsorption on the clean surface and the associated modification of the potential gradient seen by the surface/interface-state electrons show that the strength of the Rashba interaction is proportional to the effective potential gradient at the position of the surface atoms. Choosing different elements from the RE series, one can effectively vary the filling of the 4f shell that carries the magnetic moment, without modifying the outer valence-band electrons. This allows one to study the electronic structure of the surfaces with different magnetic states, and a comparison of magnetic and non-magnetic surfaces becomes possible. In the same way, practically identical surfaces of materials with very different Z-values can be addressed, enabling a study of the influence of intra-atomic spin–orbit interaction on the strength of the Rashba effect.

2. Methods

2.1. Experimental methods

Angle-resolved photoemission experiments were performed at the I-311 beamline of Max-Lab (Lund, Sweden) and at the BUS beamline of BESSYII (Berlin, Germany). The total energy resolution in these experiments was typically 30 meV, and the angular resolution was about 0.5°. The RE metal films were prepared *in situ* by metal vapor deposition on a W(110) single crystal in ultra-high vacuum. The high chemical purity and the crystalline quality of the prepared films were monitored by photoemission and low-energy electron diffraction. The formation of well-ordered, contamination-free surfaces was confirmed by monitoring the sharp surface states, which showed only minor decay on the time scale of the experiments; this is a clear indicator of the persistence of clean surfaces during the experiments.

The tungsten single crystal was mounted on a liquid-He-cooled cryostat allowing temperature variation in the range from 20 K to 2300 K. Precise temperature control was achieved with a computer-based system making use of a W–Re thermocouple. The film thickness was determined by a quartz balance monitor. The base pressure in the UHV chamber was better than 1×10^{-10} mbar rising up to 5×10^{-10} mbar during vapor deposition. Epitaxial surface monoxide layers were prepared using the recipe given in [17] with an oxygen exposure of 2 Langmuir. Photoemission experiments were performed in the geometry shown in the inset of figure 2(c). The terbium films were magnetized along their easy axis of magnetization, which is the b-direction $[10\bar{1}0]$ that coincides with the [1]–[10] direction of the W(110) substrate in case of epitaxial Tb/W(110) films (Nishiyama–Wassermann orientation). The measurements were performed on remanently magnetized films [18].

Table 1. Structural parameters of the films resulting from the calculations. The in-plane lattice constant is denoted by a_0, the interlayer relaxations d_{ij} of the first three metal layers are given in percents of the bulk interlayer spacing as determined by the c/a ratio, while the distance from the topmost metal layer to oxygen is given in Ångström.

	Tb	O/Tb	Lu	O/Lu	Y	O/Y
a_0 (Å)	3.55		3.52		3.54	
c/a	1.59		1.56		1.57	
Δd_{23}(%)	1.2	−0.8	0.5	11.3	1.1	3.6
Δd_{12}(%)	−3.0	15.7	−1.1	27.7	−3.1	22.3
d_{R-O} (Å)		0.74		0.69		0.06

2.2. Theoretical methods

Calculations of the RE metal electronic structure were performed using density functional theory (DFT) in the local-density approximation (LDA) in the form of Moruzzi *et al* [19]. For a proper description of the 4f electrons, the LDA + U method was used as described in [20], but for most cases an open-core treatment was found to be sufficient. The full-potential linearized augmented plane-wave method in film geometry [21] was applied as implemented in the FLEUR program (for program description see [22]). Spin–orbit coupling was included self-consistently in a pseudo-perturbative manner [23]. The surfaces were simulated using 12 or 14 layer films embedded in vacuum for the clean surfaces or monoxides, respectively. As in the Gd case [24], the O atoms were assumed to be adsorbed on the fcc site. While the inner six layers were kept fixed using the calculated bulk in-plane lattice parameters and c/a ratios, the upper two interlayer distances and the distance of the oxygen atoms to the underlying metal surface were allowed to relax in the calculations by minimizing the total energy. The structural parameters resulting in this way from the calculations are summarized in table 1.

The plane-wave cut-off for the basis functions was set to $k_{\max} = 3.8\,\mathrm{au}^{-1}$, and the charge density and the potential were expanded up to a cut-off of $G_{\max} = 11.5\,\mathrm{au}^{-1}$. For the metal atoms and for oxygen, the muffin-tin radius was set to 2.5 and 1.4 au, respectively. The wave function as well as the density and the potential were expanded up to $l_{\max} = 8$ inside the muffin-tin spheres. The irreducible part of the 2D Brillouin-zone (BZ) was sampled at 15 special $\vec{k}_\parallel$ points. For the calculations with spin–orbit interaction included, 41 $\vec{k}_\parallel$ points were sampled. For the *ab initio* calculations of the Tb(0001) surface including spin–orbit interaction, the magnetic moment was assumed to be oriented in the surface plane.

In the calculations, the surface was simulated by a thin film with an upper and a lower surface. Since the potential gradients on these two surfaces have opposite directions, in the case of a magnetic film, we observe Rashba splittings for the surface states on the upper and the lower surface, respectively; these represent the results of two calculations for one of these surfaces, but with opposite magnetization directions:

$$H_R^{1/2} = \alpha(\pm\vec{e}_z \times \vec{k}) \cdot \vec{\sigma} = \alpha(\vec{e}_z \times \vec{k}) \cdot (\pm\vec{\sigma}). \tag{2}$$

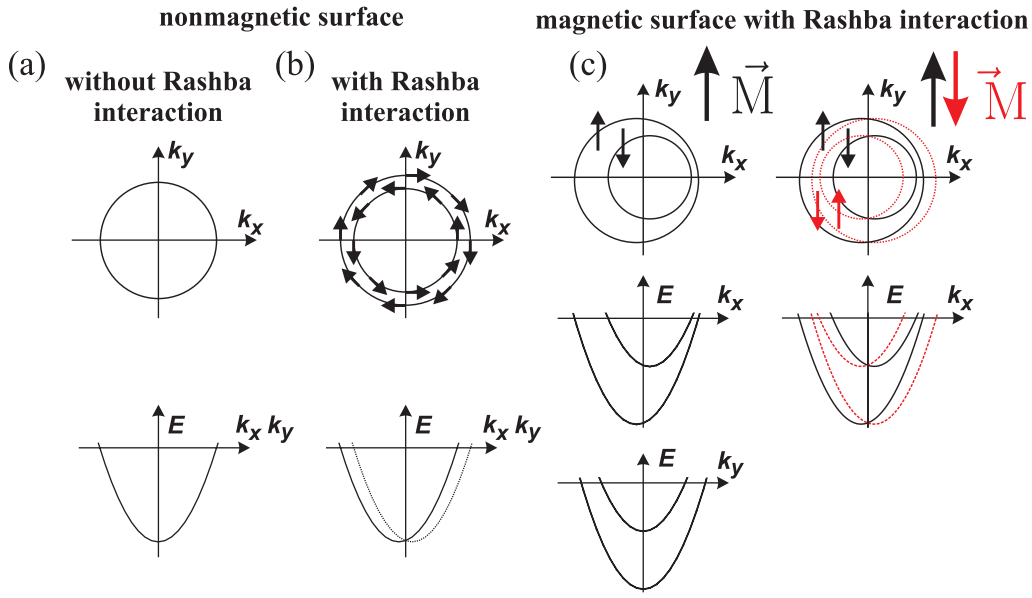

Figure 1. Schematic representations of the electronic structure of a surface state on a non-magnetic surface (a) without and (b) with Rashba spin–orbit splitting. (c) Represents the situation of a magnetic surface with exchange and Rashba splitting. The upper row shows the Fermi surfaces, the middle and lower rows display the corresponding energy-dispersion curves. The last column describes the situation when two opposite magnetization directions are analyzed (red/black).

3. Rashba interaction at magnetic and non-magnetic surfaces

Before considering the modification of the surface-state dispersions at magnetic and non-magnetic surfaces of the RE metals caused by Rashba interaction, we would like to address briefly the possible constant-energy contours that result from an intersection of the electronic bands showing Rashba interaction with the (k_x, k_y) plane of the energy–momentum space. We shall consider free-electron-gas-like bands with a simple parabolic dispersion and study the different cases that can take place at real surfaces. This will allow us to identify the essential features associated with the possible presence of a Rashba interaction at different crystal surfaces.

A natural starting point is a non-magnetic crystal surface consisting of low-Z atoms with a small intra-atomic spin–orbit contribution to the Rashba effect that will lead to a vanishing Rashba splitting. Rotational symmetry gives rise to a circular contour in the k_x–k_y plane, where the electronic bands are spin degenerate (figure 1(a)).

On a crystal surface of a non-magnetic high-Z element with a considerable intra-atomic spin–orbit interaction and an appropriate surface potential gradient, the free-electron-like parabolic dispersion will be spin split in two parabolas by the Rashba-type spin–orbit interaction (figure 1(b)). The lifting of the spin degeneracy results in two spin-polarized sub-bands with equal splitting in all azimuthal directions. In this case, the surface state has a large in-plane spin polarization, which remains always perpendicular to the electron propagation direction and the electric field. The Rashba-split states have opposite spin polarizations that rotate clockwise or counter-clockwise around the origin. The net spin polarization at the surface is evidently zero and the system remains non-magnetic.

At a surface with spontaneous magnetic order, the magnetic exchange interaction is usually much larger than the spin–orbit interaction, as seen, for example, when comparing the values of exchange splitting and Rashba splitting for terbium metal and terbium-monoxide surfaces (see below). Therefore, the spin polarization of the electronic states is defined by the exchange interaction, and all spins are aligned along a single axis. In this case, the Rashba interaction scales down from a maximum value in the $\vec{k} \perp \vec{s}$ direction to zero when $\vec{k} \parallel \vec{s}$, resulting in a reduced rotational symmetry as shown in figure 1(c). It is important to note that the exchange–split bands belong to pure spin states. Therefore, one cannot expect a co-existence of the Rashba-split pairs derived from majority or minority bands. The spin degeneracy is already removed, why only a k-dependent energy correction to the peak position is observed leading to k-dependent distortions of the majority and minority band dispersions.

The effects of a magnetization reversal on the energy bands and the constant-energy contours (marked in red) are illustrated in figure 1(c). They appear as mirror images reflected around the k_y-axis, which coincides with the magnetization direction. By superimposing the results of the two magnetization directions according to the given experimental geometry (figure 1(c), lower row), one can visualize the Rashba effect without the need of referring to a 'vanishing-Rashba geometry' and discuss it in terms of 'Rashba splitting' in analogy to the non-magnetic case.

4. Rashba interaction at magnetic RE-metal and surface-monoxide surfaces

4.1. Experiment

4.1.1. Clean Tb(0001) surface. The experimental electronic structure in the valence-band region of the Tb(0001) surface is represented in figure 2(a) by a set of energy distribution curves recorded with a constant angular shift of 0.55° between the spectra. The observed valence-band electronic structure consisting of a surface state and a T_4-bulk band is typical for heavy RE metals. The surface state is exchange split due to ferromagnetic order of terbium at low temperatures, and only its majority branch appears below the Fermi level. The surface state is rather stationary in energy near the $\overline{\Gamma}$ point and shows a downward dispersion (from the Fermi level) off the $\overline{\Gamma}$ point in the $\overline{\Gamma} \rightarrow \overline{\mathrm{K}}$ direction. The high-spin component of the 4f final-state multiplet of Tb splits into a surface and a bulk component and appears also in the valence-band region [24].

The effect of magnetization reversal on the peak position of the Tb(0001) surface state is illustrated in figure 2(b). The pairs of spectra recorded for opposite magnetization directions at normal emission and at an electron-emission angle of 2.75° (with respect to the surface normal) reveal a tiny shift of the peak position of the surface state only for off-normal emission, but no shift for normal emission.

A systematic mapping of the energy dispersion of the surface state for the $\overline{\Gamma} \rightarrow \overline{\mathrm{K}}$ direction is shown in figure 2(c), upper panel, where a distinctly different dispersion for the two opposite magnetization directions in the chosen experimental geometry is observed. Keeping in mind that the spin orientation of the surface state at a magnetic surface is defined by the magnetization direction, the latter was chosen to be orthogonal to the electron momentum $\vec{k}$ in order to maximize the Rashba interaction (see equation (1)). Although the two branches of the surface-state dispersion corresponding to opposite magnetization directions do not exist simultaneously, one can visualize the Rashba effect at a magnetic surface by superimposing the results of two

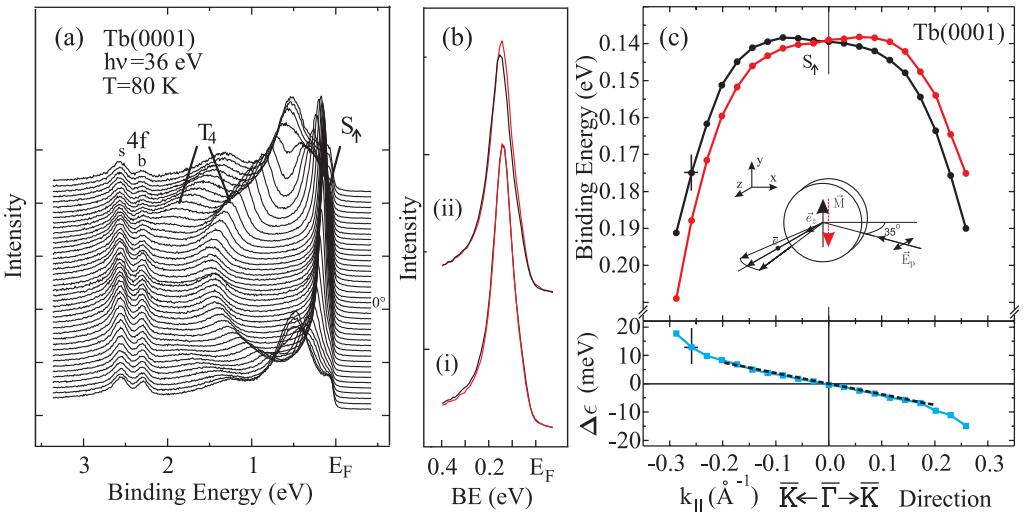

Figure 2. (a) Set of energy-distribution curves recorded in the valence-band region of the Tb(0001) surface with angular steps of 0.55° between consecutive spectra, showing the majority part of the surface state, the exchange-split T_4 band, and the shallowest 4f-multiplet component, split into surface, $4f_s$, and bulk, $4f_b$, features. (b) The Rashba effect upon magnetization reversal on the Tb(0001) surface causes a shift of the peak position (red and black curves) only in the off-normal photoemission spectra: (i) 0° (normal emission), (ii) 2.75° (off normal). (c) Dispersion of surface state on Tb(0001) at 80 K for two opposite in-plane magnetization directions (upper panel, red and black curves), and energy difference, $\Delta\varepsilon$, between the two dispersion curves of the upper panel, together with a linear fit to the data (lower panel).

subsequent experiments in a given experimental geometry that provides limiting cases for the Rashba interaction. In this way, there is no need to refer to 'vanishing Rashba' geometry, and one can discuss the results in terms of 'Rashba splitting', in analogy to a non-magnetic surface. Though the overall Rashba splitting obtained in this way for the clean Tb(0001) surface is not large, it is clearly resolvable. Similar to the behavior observed on the Gd(0001) surface [24], this behavior clearly indicates the presence of a small correction to the energy resulting from the Rashba spin–orbit interaction term.

The energy difference between the peak positions as a function of the electron momentum is plotted on the lower panel of figure 2(c). It reveals a linear dependence in the vicinity of the $\overline{\Gamma}$ point, quite similar to the case of a 2D-electron gas with Rashba interaction.

To further support and complete the description of the surface-state dispersion and its dependence on the orientation of magnetization in terms of a Rashba interaction, it would be highly instructive to investigate opposite spin orientations simultaneously in one experiment, i.e. to perform a photoemission experiment on a surface where both minority and majority states are located below the Fermi level. Fortunately, such a situation can indeed be realized on the terbium surface by adsorption of one monolayer of oxygen.

4.1.2. The $p(1 \times 1)O/Tb(0001)$ surface monoxide. Adsorption of oxygen on (0001) surfaces of trivalent RE metals leads to the formation of p(1 × 1)O/RE(0001) structures [17]. This is accompanied by a strong modification of the surface electronic structure, in particular by

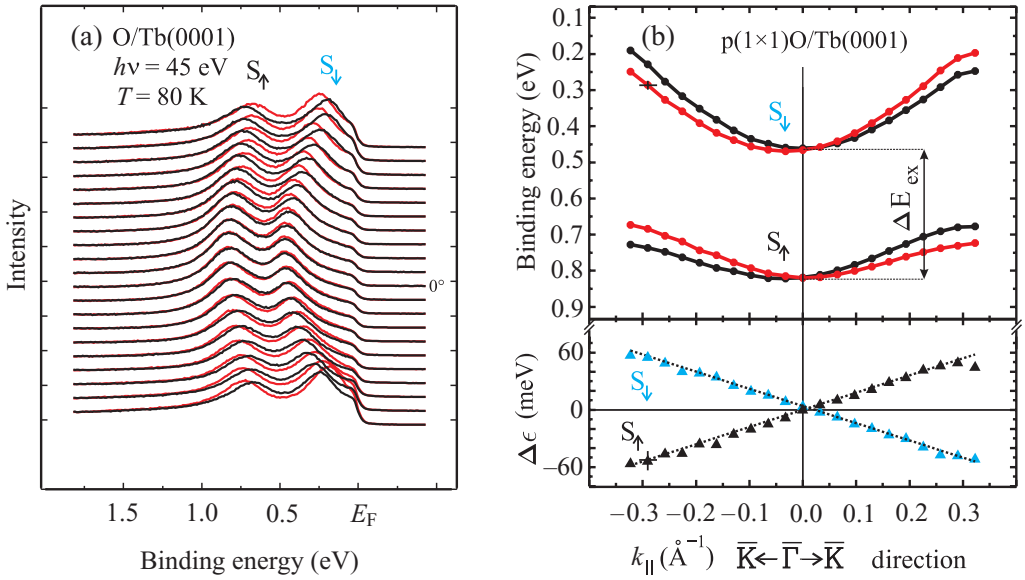

Figure 3. (a) Energy-distribution curves of p(1 × 1)O/Tb(0001), recorded in the direction of the $\overline{\mathrm{K}} \leftarrow \overline{\Gamma} \rightarrow \overline{\mathrm{K}}$ azimuth in angular steps of 0.55° between the spectra, for two opposite in-plane magnetization directions (red and black spectra). The surface/interface state is exchange-split into majority (S ↑) and minority (S ↓) components. (b) Derived energy-dispersion curves for the majority and minority components of the oxygen-induced surface/interface state on p(1 × 1)O/Tb(0001) (upper panel). The effects of magnetization reversal on the dispersion curves are clearly visible. In the lower panel, the resulting Rashba spin–orbit splitting of the majority and minority components of the surface/interface state is plotted; these were obtained from the energy dispersion curves shown in the upper panel as differences in the energies measured for the same k value, but for opposite magnetization directions.

changes in energy position and dispersion of the surface state. The surface-state band of the surface monoxide phase originates from hybridization of RE electrons with O-2p states, i.e. it can be considered to be an interface state. Owing to the increase of the binding energy of this surface/interface state in comparison to the pure RE metal, both majority and minority components become occupied and can thus be studied by photoemission. It is possible to perform experiments on magnetic surfaces, where the opposite spin polarization of majority and minority bands leads to shifts in opposite directions, providing direct evidence for the connection between spin orientation of the propagating electron and sign of the energy shift due to the Rashba effect.

The valence-band electronic structure of the p(1 × 1)O/Tb(0001) overlayer is shown in figure 3(a) by a set of energy-distribution curves covering the investigated region with constant angular steps that were recorded for two opposite magnetization directions. Both the minority and the majority branches of the exchange–split interface state are now below the Fermi level; they exhibit an upward dispersion, with the minority band having a significantly larger curvature (corresponding to a smaller effective mass). Due to magnetic exchange interaction, they have well-separated binding-energy minima of 0.47 eV (minority) and 0.82 eV (majority).

Already from an inspection of the raw data displayed in figure 3(a), the Rashba spin–orbit interaction is clearly recognizable. At the $\overline{\Gamma}$ point (normal emission), the position of the exchange–split oxygen-induced interface state is not influenced by the direction of magnetization. For off-normal emission, on the other hand, the peak position is obviously spin dependent. At a given wave vector, the peaks of the majority and minority branches shift in energy in opposite directions for each magnetization direction. Also a sign change of the $\vec{k}$ vector reverses the shifts of the interface-state peaks (indicated by the color change in the pairs corresponding to symmetrical $\vec{k}$ values). This strongly supports the conclusion that this behavior is caused by Rashba spin–orbit interaction. The shift of the majority band due to Rashba effect has the opposite sign with respect to the one observed for the clean surface indicating that the Rashba constant reverses its sign upon oxygen adsorption.

Figure 3(b) displays the dispersion of the interface state of p(1 × 1)O/Tb(0001) along the $\overline{\Gamma} \rightarrow \overline{\mathrm{K}}$ direction, as derived from the experimental data. In close analogy to the p(1 × 1)O/Gd(0001) case [24], these exchange–split interface-state bands shift considerably with respect to the center of the BZ when the magnetization direction is reversed (see black and red filled dots in figure 3(b)); at the same time, the shift is opposite for $S_{\uparrow}$ and $S_{\downarrow}$, as expected from the triple-vector product in equation (1).

An interesting question concerns the magnetic structure of the surface monoxide layer and the role that is played by the underlying ferromagnetically ordered bulk concerning the spin polarization of the oxygen-induced states. The results of a 4f core-level analysis with magnetic linear dichroism reveal that the surface monoxide layer formed on the Tb(0001) surface is not ferromagnetically ordered, in contrast to the underlying subsurface terbium layer [26]. This means that the spin polarization of the oxygen-induced interface state is driven by the subsurface terbium layer.

The energy difference, $\Delta\varepsilon$, between states of equal momentum and opposite spin orientations is plotted separately for $S_{\uparrow}$ and $S_{\downarrow}$ in figure 3(b) (lower panel). The splitting is by about a factor of five larger than that observed for the clean metal surface, showing values up to 60 meV in the interval $|k| \leqslant 0.3\,\text{Å}^{-1}$. It changes linearly as a function of k, in agreement with expectations, since this behavior is quite similar to the dispersion of the states at p(1 × 1)O/Gd(0001). However, in case of p(1 × 1)O/Tb(0001), the derived absolute values of the Rashba splitting of the majority and the minority state are obviously the same (modulo sign; see figure 3(b)). This shows that there is no connection between the strength of the dispersion and the value of the Rashba splitting.

4.2. Theory

4.2.1. Clean Tb(0001) surface. In order to unravel the mechanism leading to the increase of the Rashba interaction and the sign change of the Rashba constant upon formation of surface monoxide on the Tb(0001) surface, we compared our experimental data with the results of the DFT band-structure calculations.

Figure 4(a) shows the calculated surface-state dispersion of Tb(0001), with the surface state located in the gap of the projected bulk band structure around $\overline{\Gamma}$. The calculated band dispersions are in very good quantitative agreement with experiment (see figure 2(c)). Furthermore, the size of the Rashba splitting agrees well with the experimental data.

Figure 4(c) displays charge-density profiles of the occupied majority-spin surface states of the Tb(0001) surface. Here, the shapes of the charge-density contour lines clearly reveal

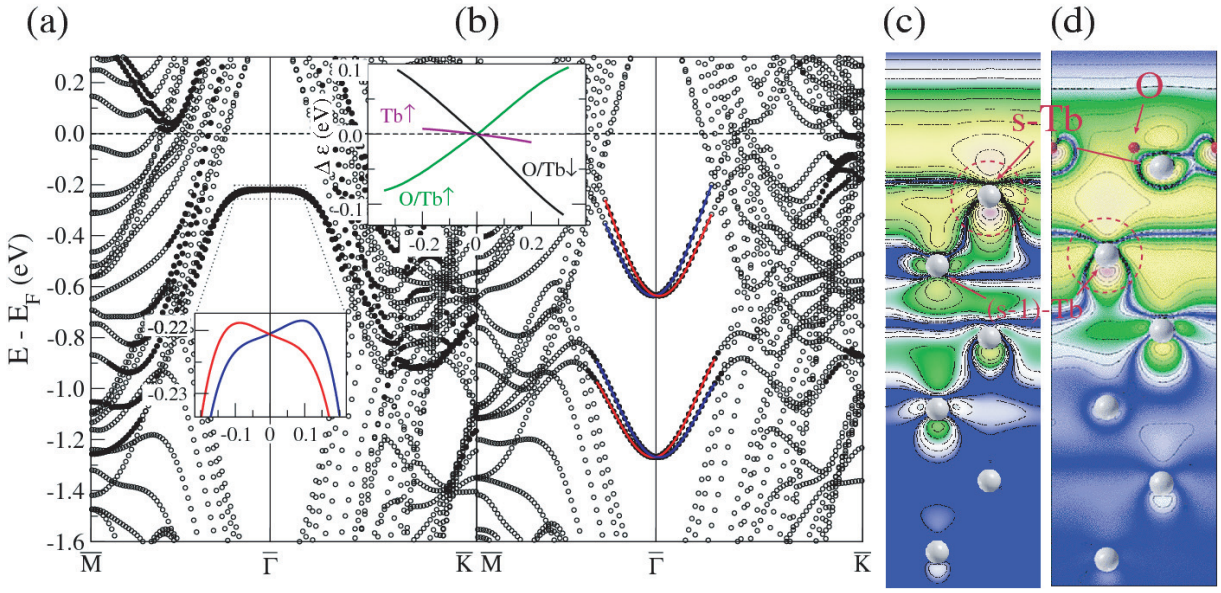

Figure 4. Electronic band structures of (a) Tb(0001) and (b) p(1 × 1)O/Tb(0001) from DFT calculations. In inset (i), the Rashba splittings of the majority and minority components of the surface state on Tb(0001), obtained from these theoretical results, are shown around $\overline{\Gamma}$, in strong magnification. In (b), the magnetic-exchange splitting and the Rashba splitting of the interface state on p(1 × 1)O/Tb(0001) are clearly visible. In both cases, the two branches (red and blue) correspond to opposite magnetization directions. Inset (ii) shows the Rashba splitting of the majority and minority components of the interface state on p(1 × 1)O/Tb(0001), obtained as differences between the dispersion curves for a given $\vec{k}_{\|}$ value and opposite magnetization directions. For comparison, the Rashba splitting of the surface state on Tb(0001) is also plotted. (c) and (d) Charge-density contour plots of the majority parts of the surface/interface state in a plane perpendicular to the surface for (c) clean Tb(0001) and (d) the p(1 × 1)O/Tb(0001) surface. The plot represents a cross section through the center of the film cutting through six Tb atoms. Changes of charge densities are shown by color changes (log scale) from red (high density) to blue (low density).

the d_{z^2}-symmetry of the surface state. The strong surface localization is quite remarkable; as is the large fraction of the surface state that extends into the vacuum region. The LDA calculations show that over 70% of the charge density of the surface state is located in the surface layer and the vacuum region, and that it has mainly 5d-character inside the surface muffin-tin sphere. Hence, the interaction with the sub-surface layer and the underlying Tb bulk is rather small. This argument is further substantiated by the very weak dependence of the surface-state binding energy (minority and majority parts) on interlayer relaxation and also on the type of close-packed stacking of the surface layer (fcc versus hcp) as observed on the Gd surface [20].

4.2.2. The $p(1 \times 1)O/Tb(0001)$ surface monoxide. The electronegative oxygen atoms, adsorbed on the terbium surface, have a strong effect on the entire near-surface charge distribution (figures 4 (c) and (d)) and subsequently on the energy dispersion of the interface state. In good agreement with the experimental data presented in figure 3(b), we find two occupied states dispersing upwards, the minority state, located at -0.7 eV relative to the Fermi level (at the $\overline{\Gamma}$-point), and the majority state at -1.3 eV. The exchange splitting amounts to 0.64 eV, i.e. it is 0.29 eV larger than the experimentally observed value; a similar overestimation of the exchange splitting had also been found in the calculations for Gd(0001) metal [20]. The Rashba splitting of the interface states is calculated to be about five times larger than that of the surface state on the Tb(0001) metal surface, in good agreement with experimental observation. In the surface Tb layer, the local valence moment is three times smaller than in the subsurface layer, consistent with the observation that the spin polarization of the oxygen-induced interface state is sustained by subsurface Tb.

The changes in the charge-density contours of the surface state upon oxygen adsorption are quite remarkable, as shown in figure 4(d). The characteristic charge contour of the majority and the minority parts of the interface state for p(1 × 1)O/Tb(0001) resides no longer in the surface (s-Tb) layer, as it does in the case of the metal surface, but shifts to the subsurface layer, (s-1)-Tb. This is the reason why this state should be considered an interface state rather than a surface state, where the former is located between the bulk Tb metal and the surface monoxide p(1 × 1)O/Tb(0001) layer. Also, most of the charge density from the vacuum region (amounting to 40% in case of Tb(0001)) is drawn towards the surface layer and below (only 6% remains in the vacuum region).

The calculations also show that upon oxide-layer formation there is a redistribution of the orbital character of the states near the $\overline{\Gamma}$-point inside the terbium muffin-tin sphere. In agreement with the results of resonant photoemission experiments [17], the calculations indicate a strong contribution of the oxygen sp-electrons to the surface state. The orbital character of the topmost Tb atom changes from almost pure d-like for the clean surface to one with substantial admixture of s character, as well as some p contributions in the O-covered system. The relative weights of electrons with different orbital characters in the first layer (inside the muffin-tin spheres) change from $s : p : d = 0 : 11 : 89$ for elemental Tb(0001) to $65 : 13 : 17$ for p(1 × 1)O/Tb(0001). In the second Tb layer, these weights change from $s : p : d = 8 : 1 : 90$ to $5 : 14 : 81$. While in clean Tb, the charge of the surface state is mainly localized on the surface atom, in O/Tb this weight is shifted to the subsurface Tb. Accordingly, on the Tb (0001) surface, the electronic charge distribution resembles the symmetric shape of a d_{z^2}-orbital, while upon oxidation, this state becomes rather asymmetric.

4.2.3. Modification of Rashba interaction through oxidation. By locally switching on or off the spin–orbit contribution to the Hamiltonian of the muffin tins, we can obtain the layer-resolved Rashba spin–orbit contributions. From this, one can see that in the case of the clean Tb(0001) surface, the first layer provides the main contribution (about two thirds) of the total splitting; while the second layer contributes only about one quarter. In the surface-monoxide case, the situation changes dramatically, since the main contribution to the splitting arises now from the subsurface (s-1) layer, whereas the third layer contributes only 15%. The contribution from the topmost Tb atom is almost negligible. These findings correspond well to the changes in the orbital character (as will be discussed below) and to the occupation of the muffin-tin spheres around the atoms at these surfaces.

The observation of an increase of the Rashba splitting through oxygen adsorption on Tb(0001) can be further understood using qualitative arguments from atomic physics [27] as well as the results of a tight-binding model [14]. The latter allows one to identify the main contributions to a sizeable Rashba effect at the surface, which are—in addition to the gradient of the surface potential—the atomic spin–orbit interaction and the orbital characters of the wave functions involved.

4.2.4. Atomic spin–orbit interaction. In the subsurface (s-1) layer of the surface monoxide, the contribution of the p states is enhanced as compared with the clean terbium surface. In a free atom, the spin–orbit splitting of electronic levels is well known and can be described by $H_{\mathrm{SOC}} = (Z_{\mathrm{eff}}^4/n^3)(1/l(l+1))$. The factor Z_{eff}^4/n^3 can be estimated for the terbium atom, but it is difficult to use this expression for describing changes due to bonding between oxygen and terbium. However, using this expression, we estimate the effect of p-state admixture to a spin–orbit split d-state: $1/\mathrm{l}(\mathrm{l}+1)$ changes from $1/6$ to $1/2$ when going from a pure d to a pure p state. Keeping n constant, this would lead to an increase of the Rashba splitting by a factor of 3 (in our rather crude central-potential picture).

4.2.5. Orbital character. It was shown on the basis of the tight-binding model that besides atomic spin–orbit interaction, the asymmetry of the electronic charge distribution of the surface state is an important condition for the Rashba effect to occur [14], and it can serve as a sensor for the effective coupling between Rashba and atomic spin–orbit interaction terms.

In a tight-binding model, the breaking of inversion symmetry leads to an admixture of p_x and p_y bands lying in the (x, y)-surface plane to the p_z state (representing the surface state). The resulting asymmetric charge distribution of the electron cloud with respect to the (x,y) plane results in a nonzero overlap matrix element (hopping parameter) between p_z and the $(\mathrm{p}_x, \mathrm{p}_y,)$ orbitals. Since in this model, the Rashba parameter is given by the product of an averaged atomic spin–orbit coupling parameter and this hopping term, it is crucial that both quantities are nonzero to yield a strong Rashba effect: without broken inversion symmetry, the inversion $z \rightarrow -z$ would lead to an equally large overlap of the $(\mathrm{p}_x, \mathrm{p}_y)$ orbital with the positive and negative lobes of p_z, with the result that the hopping parameter would vanish. One can use this result of the tight-binding model as a qualitative argument when discussing real systems.

The importance of the shape of the wave function has also been proven by LDA + U calculations for the surface state on Lu(0001) [28]. It has been shown that at different points $(\overline{\Gamma}, \overline{\mathrm{M}})$ of the surface BZ, the symmetry of the surface state is different. The charge distribution at the $\overline{\Gamma}$ point is practically symmetric, while it is strongly deformed at the $\overline{\mathrm{M}}$ point; the corresponding band structure shows a very small Rashba splitting at $\overline{\Gamma}$ and a sizeable effect at the $\overline{\mathrm{M}}$ point.

In good agreement with our observation of an increased Rashba splitting of the surface/interface state caused by oxygen adsorption, figure 4(d) reveals a strong deformation of the electronic cloud at the $\overline{\Gamma}$ point for $\mathrm{p}(1 \times 1)\mathrm{O/Tb}(0001)$, but a practically symmetric distribution for the majority surface state of the clean surface, figure 4(b). These examples allow us to conclude that the shape of the electronic charge cloud is an important parameter for the size of the Rashba effect.

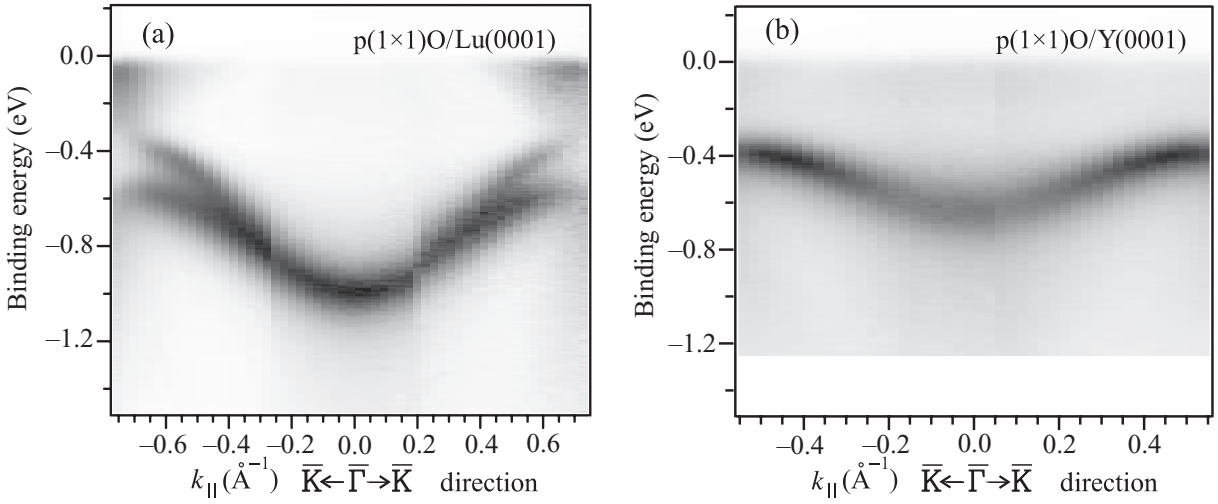

Figure 5. (a) Experimental interface-state dispersion for p(1 × 1)O/Lu(0001) at $T = 80$ K shown as an intensity plot, where dark grays correspond to high photoemission intensities. The interface state is split into two branches by the Rashba spin–orbit interaction. (b) Same for p(1 × 1)O/Y(0001) at $T = 80$ K, however with no resolvable splitting in this case.

5. Rashba interaction at the non-magnetic surface monoxides of lutetium and yttrium

Although photoemission is not well suited to study the behavior of the surface states at the clean (0001) surfaces of non-magnetic RE metals as they are located too close to the Fermi level or above it (see e.g. [15, 16]), oxygen adsorption leads to an increase of the surface-state binding energy and makes such experiments feasible. As the result of a mixing of the O–2p states with d-electrons of the outer shells of the RE metals, the interface states of the monoxides are very similar along the RE series and allow a direct comparison between them at surfaces of different RE metals.

Similar to the terbium case considered above, one can prepare surface monoxides on the surfaces of lutetium and yttrium metal. This allows us to address the influence of the Rashba interaction on the electrons localized at the oxide/metal interface with non-magnetic RE-metal surfaces. The yttrium and lutetium surfaces are particularly attractive, since both are non-magnetic, but exhibit a large difference in their Z-values: $Z = 39$ for yttrium and $Z = 71$ for lutetium. In this way, a contribution of the intra-atomic spin–orbit interaction to the Rashba effect is effectively 'turned-on' for lutetium and 'turned-off' for yttrium.

The dispersions of the interface states at the p(1 × 1)O/Lu(0001) and p(1 × 1)O/Y(0001) surfaces are displayed in figures 5(a) and (b). The interface states disperse upwards, i.e. similar to the case of terbium monoxide, but they are not split by exchange interaction. Therefore, in both cases, only one peak associated with the spin degenerate state is observable at the $\overline{\Gamma}$ point.

Tracking the peak behavior along the $\overline{\Gamma} \rightarrow \overline{\mathrm{K}}$ direction at the p(1 × 1)O/Lu(0001) surface, one observes a continuous change of the width and shape of the peak, resulting finally in a splitting into a double-peak structure (see figure 5(a)). The value of the splitting varies linearly with wave vector $\vec{k}$ reaching a maximum value of ∼200 meV at $|k| = 0.65$ Å^{-1}, before the peaks disappear due to the loss of localization in the region where the projected bulk band gap closes

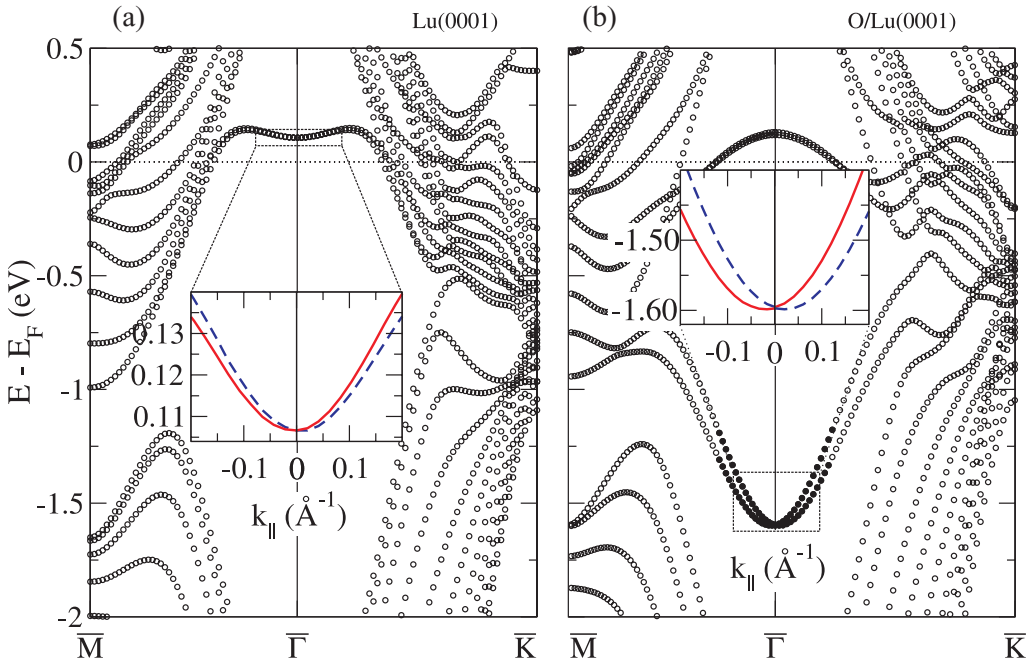

Figure 6. Electronic band structure of (a) Lu(0001) and (b) p(1 × 1)O/Lu(0001) from DFT calculations. The Rashba splitting of the surface/interface state around the $\overline{\Gamma}$ point is again plotted for the two cases in the insets on magnified scales. Again, the two branches (red solid and blue dashed) correspond to opposite spin polarizations of the surface/interface states.

and the surface-state band overlaps with the bulk bands. The behavior of the interface state resembles the behavior observed for the sp-like surface state of Au(111), providing further proof that the Rashba effect influences the oxygen-induced interface state on RE metals.

In contrast to this, an examination of the dispersion of the interface state on the p(1 × 1)O/Y(0001) surface reveals no evidence for a Rashba splitting (see figure 5(b)). Considering similar values for the surface-potential gradient at the lutetium and yttrium surfaces, it becomes clear that the considerable intra-atomic spin–orbit interaction of the Lu atoms is an essential contribution to the Rashba spin–orbit interaction, since without such a contribution at the yttrium surface the Rashba interaction vanishes. This provides direct evidence of the close connection between the value of the intra-atomic spin–orbit interaction of the atoms present at a given surface and the strength of the Rashba effect that can be observed on it.

The results of electronic band-structure calculations of the Lu(0001) and p(1 × 1)O/Lu(0001) surfaces are presented in figures 6(a) and (b). The most interesting feature in the electronic band structure is the surface/interface state located in the gap of bulk bands around the $\overline{\Gamma}$-point. At the clean surface, the surface state is located at ∼105 meV above the Fermi level and shows a slight upwards dispersion at the $\overline{\Gamma}$-point, which turns down when the surface state approaches the edge of the projected bulk bands [28]. The points of dispersion with more than 90% of charge localized in the vacuum region and the surface layer are shown by filled circles. Upon formation of surface monoxide, the electronic band structure changes and the surface state shifts down considerably to higher binding energies, i.e. it turns to an interface state (it is located at 1.6 eV binding energy), and shows considerably stronger upward dispersion. This behavior

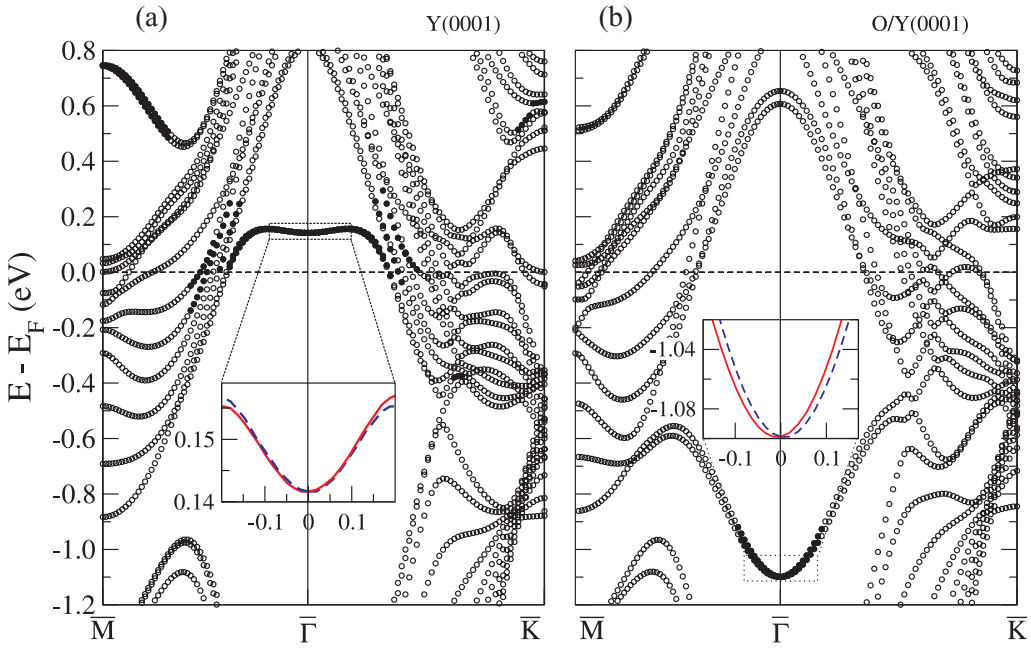

Figure 7. Electronic band structures of (a) Y(0001) and (b) p(1 × 1)O/Y(0001) from DFT calculations. The insets zoom into the regions around the $\overline{\Gamma}$ point revealing an almost vanishingly small Rashba splitting in both cases. The two branches (red and blue) correspond to opposite spin polarizations of the surface/interface states.

agrees well with the experimental data, although the energy positions of the surface/interface-state minima deviate from the experimental values of ∼0 eV [29] and 1 eV for the clean and oxygen-covered surfaces, respectively.

In good agreement with the experimental data, the Rashba splitting is found to reach ∼200 meV at $|k| = 0.6\,\text{Å}^{-1}$ for the surface-monoxide system. Calculations for the clean surface predict only ∼5 meV splitting at $|k| = 0.2\,\text{Å}^{-1}$. Such a small splitting cannot be resolved in our experiments on the clean surface even if the states were below the Fermi level. Nevertheless, the calculations show that at the $\overline{\text{M}}$-point, the surface state of the clean Lu(0001) surface is characterized by a considerable splitting [28]; this difference can be understood if one considers the shapes of the electronic charge distribution at the $\overline{\Gamma}$- and $\overline{\text{M}}$-points in a way similar as discussed above for the clean and oxygen-covered Tb(0001) surfaces.

Figures 7(a) and (b) present the calculated electronic band structures of Y(0001) and p(1 × 1)O/Y(0001), respectively. The overall electronic structures are very similar to those obtained for Lu(0001) and p(1 × 1)O/Lu(0001). The surface/interface-state dispersions have similar shapes and the minima are located at 142 meV above the Fermi level for clean yttrium and at 1.1 eV below the Fermi level for the surface monoxide. Similar to the previous case, these values deviate from the corresponding binding energies of 0 and 0.63 eV, respectively. But the main difference appears in comparison to the splitting of the surface/interface states on Lu(0001) and p(1 × 1)O/Lu(0001). In contrast to the latter case, the surface state reveals no splitting on the clean yttrium surface, while the interface state on the oxygen-covered yttrium surface shows a very small splitting (<5 meV). This agrees with our expectation based on the

small Z-value of yttrium and the discussion about the intra-atomic spin–orbit contribution to the Rashba interaction.

The surfaces of p(1 × 1)O/Y(0001), p(1 × 1)O/Lu(0001), Tb(0001) and p(1 × 1)O/Tb(0001) considered above present nice examples that demonstrate the role of spin–orbit interaction at the three types of surfaces discussed in section 3.

6. Comparison with magnetic linear dichroism

Finally, we want to point out that the experimental conditions used in our experiments on the magnetic surfaces are identical to those used in experiments on magnetic dichroism using linearly polarized light. To avoid confusion, we shall briefly address the seemingly close relationship between the Rashba effect and magnetic linear dichroism in photoemission. Both effects are consequences of spin–orbit interaction and show up in systems with broken inversion symmetry. However, the relevant physical quantities defining the symmetry are different. The Rashba effect scales with the triple-vector product in equation (1) between the electric field direction, the electron wave vector and the electron spin, which are all properties of the electronic ground state. By contrast, magnetic linear dichroism in angle-resolved photoemission is not a ground-state property of the system, but it is observed in electric dipole transitions as intensity changes of photo-excited electrons due to variations of the transition probabilities from initial to final states when measuring in a so-called *chiral* geometry [30]. The chiral geometry in a magnetic-linear-dichroism experiment is given by the different non-vanishing triple-vector product spanned by the polarization vector of the incoming light, the wave vector of the outgoing photoelectron, and its spin. The Rashba splittings in the present experiments can also be measured using s-polarized light (light polarization vector aligned in the direction of magnetization), i.e. using a non-chiral geometry in which magnetic linear dichroism cannot occur. And vice versa, one can observe magnetic linear dichroism even when the Rashba effect vanishes for symmetry reasons, as e.g. in photoemission from bulk bands of cubic crystals. From a practical point of view, the Rashba effect appears in experiments as a change in energy positions $E(\vec{k}_{\parallel})$ of surface-state peaks for opposite magnetization directions, while changes in the intensities of photoemission lines must be attributed to magnetic dichroism.

7. Summary and conclusions

In this work, we presented a detailed investigation of the surface states at the surfaces of magnetic and non-magnetic RE metals, providing experimental and theoretical evidence for the Rashba effect. We demonstrated that the Rashba effect leads to a dependence of the energy dispersions of the surface state on Tb(0001) and the interface state on p(1 × 1)O/Tb(0001) on the direction of magnetization, and also to a splitting of the interface state on the non-magnetic p(1 × 1)O/Lu(0001) surface. In addition, we showed that the Rashba interaction is negligibly small at the p(1 × 1)O/Y(0001) surface due to the small intra-atomic spin–orbit interaction in this case. We demonstrated that the strength of the Rashba effect can be changed, e.g. by oxygen adsorption, which leads to a strong modification of the near-surface electronic structure and in this way to an increased spin splitting. Using the calculated charge-density contours and weights of the different orbitals contributing to the surface/interface states, we were able to identify the most important contributions to the observed enhancement of the Rashba effect upon formation of the surface-oxide layer. In particular, we showed that the magnitude of the effect

is controlled by the atomic contribution to the potential gradient experienced by the electronic states, by the shape of the electronic charge-density distribution, and by the hybridization of the electronic states located at the surface/interface. On the example of simple parabolic bands, we discussed the differences between the constant-energy contours resulting from the Rashba effect at non-magnetic and magnetic surfaces, and we pointed out the difference between the Rashba effect and the magnetic linear dichroism in photoemission that can be observed under similar experimental conditions.

Acknowledgments

Financial support through Deutsche Forschungsgemeinschaft, projects STA 413/3–1, BI 823–1/1 and SfB-290/TP6, is gratefully acknowledged. This work was also supported by the US DOE under grant DE-FG02-04ER46158. The Advanced Light Source is operated under US DOE contract DE-AC03-76SF00098 at Lawrence Berkeley National Laboratory. JEP acknowledges financial support by the A-v-Humboldt foundation and by the MEC program 'Ramón y Cajal'. We gratefully acknowledge Christian Schüßler-Langeheine for designing and setting up the photoemission endstation used during the experiments at BessyII.

References

[1] Rashba E I 1960 *Sov. Phys. Solid State* **2** 1109
[2] Winkler R 2003 *Spin–Orbit Coupling Effect is Two-Dimensional Electron and Hole Systems (Springer Tracts in Modern Physics* vol 191*)* (Berlin: Springer)
[3] Zutic I, Fabian J and Sarma S D 2004 *Rev. Mod. Phys.* **76** 323
[4] Awschalom D D, Loss D and Samarth N 2002 *Semiconductor Spintronics and Quantum Computation* (Berlin: Springer)
[5] Fabian J, Matos-Abiague A, Ertler C, Stano P and Zutic I 2007 *Acta Phys. Slovaca* **57** 565
[6] LaShell S, McDougall B A and Jensen E 1996 *Phys. Rev. Lett.* **77** 3419
[7] Rotenberg E and Kevan S D 1998 *Phys. Rev. Lett.* **80** 2905
[8] Hochstrasser M, Tobin J G, Rotenberg E and Kevan S D 2002 *Phys. Rev. Lett.* **89** 216802
[9] Koroteev Yu M, Bihlmayer G, Gayone J E, Chulkov E V, Blügel S, Echenique P M and Hofmann Ph 2004 *Phys. Rev. Lett.* **93** 046403
[10] Ast C R, Henk J, Ernst A, Moreschini L, Falub M C, Pacilé D, Bruno P, Kern K and Grioni M 2007 *Phys. Rev. Lett.* **98** 186807
[11] Koitzsch C, Battaglia C, Clerc F, Despont L, Garnier M G and Aebi P 2005 *Phys. Rev. Lett.* **95** 126401
[12] Shikin A M, Varykhalov A, Prudnikova G V, Usachov D, Adamchuk V K, Yamada Y, Riley J D and Rader O 2008 *Phys. Rev. Lett.* **100** 057601
[13] Dedkov Yu S, Fonin M, Rüdiger U and Laubschat C 2008 *Phys. Rev. Lett.* **100** 107602
[14] Petersen L and Hedegard P 2000 *Surf. Sci.* **459** 49
[15] Wegner D, Bauer A and Kaindl G 2006 *Phys. Rev.* B **73** 165415
[16] Fedorov A V, Hohr A, Weschke E and Starke K 1994 *Phys. Rev.* B **49** 5117
[17] Schüssler-Langeheine C, Meier R, Ott H, Hu Z, Mazumdar C, Grigoriev A Y, Kaindl G and Weschke E 1999 *Phys. Rev.* B **60** 3449
[18] Heigl F, Prieto J E, Krupin O, Starke K, Kaindl G and Bode M 2005 *Phys. Rev.* B **72** 035417
[19] Moruzzi V, Janak J and Williams A 1978 *Calculated Electronic Properties of Metals* (New York: Pergamon)
[20] Kurz P, Bihlmayer G and Blügel S 2002 *J. Phys.: Condens. Matter* **14** 6353
[21] Wimmer E, Krakauer H, Weinert M and Freeman A J 1981 *Phys. Rev.* B **24** 864
[22] http://www.flapw.de

[23] Li C, Freeman A J, Jansen H J F and Fu C L 1990 *Phys. Rev.* B **42** 5433
[24] Krupin O, Bihlmayer G, Starke K, Gorovikov S, Prieto J E, Döbrich K, Blügel S and Kaindl G 2005 *Phys. Rev.* B **71** 201403
[25] Navas E, Starke K, Laubschat C, Weschke E and Kaindl G 1993 *Phys. Rev.* B **48** 14753
[26] Krupin O 2004 *Dissertation* Free University Berlin http://www.diss.fu-berlin.de/2004/249/indexe.html
[27] Demtroeder W 2000 *Experimentalphysik 3* (Berlin: Springer)
[28] Bihlmayer G, Koroteev Yu M, Echenique P M, Chulkov E V and Blügel S 2006 *Surf. Sci.* **600** 3888
[29] Wegner D, Bauer A, Koroteev Yu M, Bihlmayer G, Chulkov E V, Echenique P M and Kaindl G 2006 *Phys. Rev.* B **73** 115403
[30] Feder R and Henk J 1996 *Spin–Orbit Influenced Spectroscopes of Magnetic Solids* vol 466 (Berlin: Springer)